Diffusion-Controlled Anisotropic Growth of Stable and Metastable Crystal Polymorphs in the Phase-Field Crystal Model

G. Tegze,[1] L. Gránásy,[1] G. I. Tóth,[2] F. Podmaniczky,[2] A. Jaatinen,[3,4] T. Ala-Nissila,[3,*] and T. Pusztai[2]

[1]*BCAST, Brunel University, Uxbridge, Middlesex, UB8 3PH, United Kingdom*
[2]*Research Institute for Solid State Physics and Optics, H-1525 Budapest, Post Office Box 49, Hungary*
[3]*Department of Applied Physics, Helsinki University of Technology, Post Office Box 1100, FI-02015 TKK, Finland*
[4]*Department of Materials Science and Engineering, Helsinki University of Technology,*
Post Office Box 6200, FI-02015 TKK, Espoo, Finland

We use a simple density functional approach on a diffusional time scale, to address freezing to the body-centered cubic (bcc), hexagonal close-packed (hcp), and face-centered cubic (fcc) structures. We observe faceted equilibrium shapes and diffusion-controlled layerwise crystal growth consistent with two-dimensional nucleation. The predicted growth anisotropies are discussed in relation with results from experiment and atomistic simulations. We also demonstrate that varying the lattice constant of a simple cubic substrate, one can tune the epitaxially growing body-centered tetragonal structure between bcc and fcc, and observe a Mullins-Sekerka–Asaro-Tiller-Grinfeld-type instability.

Depending on the conditions of freezing, undercooled liquids may solidify to different crystal structures. The selection of the crystal structure is influenced by various properties of the available crystalline phases including the thermodynamic driving force of freezing, and the kinetic coefficient that describes the attachment of atoms to the surface of the crystal. An interesting question that can only be answered using an atomistic approach is, how the growth rates of stable and metastable crystalline polymorphs forming in the same liquid do compare. Molecular dynamics (MD) simulations have been used widely to evaluate the growth anisotropy of the solid-liquid interface [1]. However, in such simulations the diffusion-controlled regime cannot be easily accessed, and the realization of a multiplicity of metastable and stable phases is not without difficulties. Other promising candidates are the molecular theories of freezing that rely on the density functional technique (DFT). In the past decades a variety of DFTs have been developed [2]. However, simulation of crystal growth has became reality only recently, within a dynamical extension of the DFT (DDFT) [3]. These studies are restricted to a few hundred atoms. Starting from a simplified free energy functional, a newly emerging DDFT-type approach, known as the phase-field crystal (PFC) method [4], appears to be able to address crystalline freezing on a far larger scale.

In this Letter, we use the PFC method to compare the growth of several crystalline polymorphs in the same undercooled liquid. The reduced free energy is as follows:

$$\mathcal{F} = \int d\mathbf{r}\left\{\frac{n}{2}[B_L + B_S(2\nabla^2 + \nabla^4)]n - \frac{\upsilon n^3}{6} + \frac{n^4}{12}\right\}, \quad (1)$$

where $\mathcal{F} = (F - F_L^{\mathrm{ref}})/(\rho_L^{\mathrm{ref}}\lambda^3 k_B T)$, F_L^{ref} and ρ_L^{ref} are the

free energy and the number density of the reference liquid, λ the length scale, $n = (\rho - \rho_L^{\mathrm{ref}})/\rho_L^{\mathrm{ref}}$ the reduced number density, $B_L = (\kappa_L \rho_L^{\mathrm{ref}} k_B T)^{-1}$, and $B_S = K(\rho_L^{\mathrm{ref}} k_B T)^{-1}$. Here κ_L is the compressibility of the liquid, K the bulk modulus of the crystal, while adjusting υ, one may incorporate the 0th order contribution from three-body correlations. This form of $\mathcal{F}$ can be deduced from a perturbative DFT [2] after some simplifications [4]. This approach retains the richness of the original DFT, and predicts crystal structure, anisotropy, and elastic properties. This model is known to crystallize to the bcc structure [4]; however, any periodic structure of similar nearest neighbor distance shall be a local minimum of the free energy. Thus the PFC model is expected to be able to predict phase preference or selection.

Since n is a conserved quantity, in the overdamped limit its time evolution obeys the equation of motion

$$\frac{\partial n}{\partial t} = \nabla \cdot \left[M_n \nabla\left(\frac{\delta F}{\delta n}\right)\right], \quad (2)$$

where a constant mobility of the form $M_n = [(1 + n_0)D_\rho/(k_B T \rho_L^{\mathrm{ref}})]$ sets the time scale for system evolution, while n_0 is the reduced number density of the initial supersaturated liquid, D_ρ the self-diffusion coefficient, and $\delta F/\delta n$ is the first functional derivative of the free energy with respect to the field n [5]. An advantage of the PFC method is that it is able to address processes on the diffusive time scale, which is by orders of magnitude longer than the time accessible for other atomistic simulations, such as molecular dynamics [4]. Such diffusion-controlled relaxation dynamics is relevant for colloidal systems and for deeply undercooled liquids, where the self-diffusion of the particles is expected to be the dominant way of density relaxation. Accordingly, the present computations will be

indicative to the behavior of colloidal systems. Indeed such systems are known to crystallize to structures investigated here [6].

We assume herein $B_S = 3^{-1/2}/2$, $\Delta B = B_L - B_S = 5 \times 10^{-5}$, and $v = 3^{1/4}/2$. The respective coexistence regions between the liquid and crystalline phases obtained by a full numerical minimization of the free energy with respect to $n(\mathbf{r})$ and the common tangent construction are bcc liquid: $-0.0862 < n_0 < -0.0315$, hcp liquid: $-0.0865 < n_0 < -0.0344$, fcc liquid: $-0.0862 < n_0 < -0.0347$, and sc liquid: $-0.0249 < n_0 < 0.0216$. The driving force for crystallization (the grand potential density difference relative to the initial liquid [7]) is presented in Fig. 1. Remarkably, the driving forces for the bcc, hcp, and fcc structures are very similar (they differ by less than 7%). In the density range investigated, the sequence of phases, in decreasing order of the thermodynamic driving force, is bcc, hcp, fcc, and sc. Such preference of the bcc phase is seen in charged colloids [8].

Crystallization has been started by placing at the center of the simulation box ($L_x/2$, $L_y/2$, $L_z/2$, [9]) either (i) a sphere (for equilibrium shape) or (ii) a rectangular slab (for growth studies) filled by a fairly accurate approximation [10] of the density distribution of the bulk crystal, oriented appropriately, or (iii) a $4a_0$ thick slab of crystalline substrate (for heteroepitaxy) represented by a periodic potential term $V(\mathbf{r})n$ added to the free energy, where $V = -0.0533$ for spherical regions located on a sc lattice of lattice constant a_0, and $V = 0$ otherwise.

First, to gain information on the anisotropy of the solid-liquid interface free energy γ, we determined the (stable and metastable) equilibrium shapes (that minimize for a given cluster volume the contribution from γ and reflects its anisotropy). This has been done by growing spherical seeds until reaching equilibrium with the remaining liquid. The sc crystallite has proven unstable. We observe rhombo-dodecahedral, octahedral, and hexagonal-prism shapes for the bcc, fcc, and hcp structures, bound exclusively by the {110}, the {111}, and the {10$\bar{1}$0} and {0001} faces. This strong faceting (often seen in colloids [11]) emerges as a result of a thin crystal-liquid interface that extends to ~1–2 molecular layers. With the exception of

hcp, where $\gamma_{10\bar{1}0}/\gamma_{0001} = 1.08 \pm 0.01$, the specific crystal shape prevents us from evaluating the anisotropy of γ by the Wulff construction.

Next, we study the dislocation-free growth of the {100}, {110} and {111} faces of the bcc and fcc structures, and the {0001}, {10$\bar{1}$0}, and {11$\bar{2}$0} faces of hcp. In all these cases, we observe flat fronts. The results for the bcc structure are summarized in Fig. 2. The local number density along the centerline in the growth direction (z), and the coarse-grained density (the local average, $\tilde{n}$, obtained by FIR filtering [12] the x-y plane averaged density) are shown
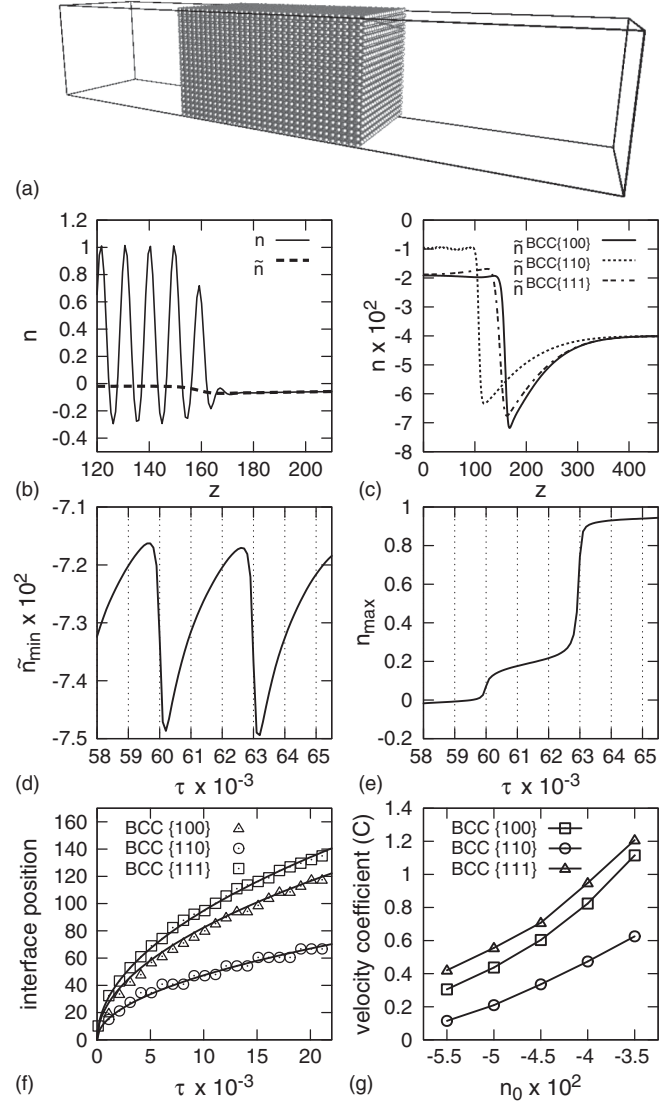
FIG. 2.   bcc crystal growth as predicted by the PFC model. (a) Simulation box with crystal growing into the (100) direction. (b) Local and coarse-grained (filtered) densities across the {100} interface. (c) Coarse-grained densities for the {100}, {110}, and {111} interfaces. (d) Depth of the depletion zone vs dimensionless time (τ) in (b). (e) Peak amplitude vs τ for (b). (f) Interface position vs τ and (g) the velocity coefficients vs n_0 for the three low index orientations.
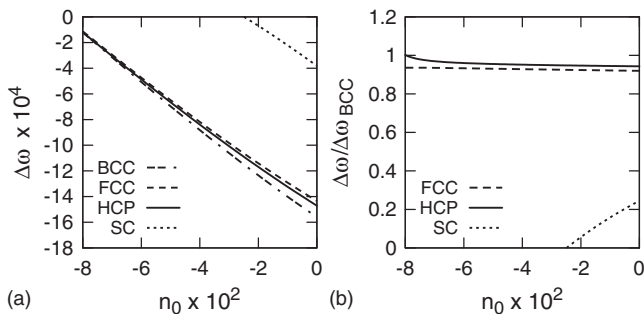

FIG. 1.   (a) Driving force of crystallization, $\Delta\omega$, and (b) $\Delta\omega/\Delta\omega_{bcc}$ vs initial number density for various polymorphs.

in Fig. 2(b) for the {100} face. The density of crystals precipitating from the same far-field liquid density (n_0) differs significantly for the individual faces [Fig. 2(c)]. These crystal densities realize the maximum driving force possible for crystal growth from the respective depleted liquid (of density $\tilde{n}_{min}$) ahead of the front. $\tilde{n}_{min}$ varies periodically with time [Fig. 2(d)], indicating a barrier-controlled layerwise growth process, presumably via 2D nucleation, consistently with the faceted morphology. The sharp drops in $\tilde{n}_{min}(\tau)$ correspond to the formation of new layers. Forming of a crystal plane is monitored by the amplitude of the respective density peak n_{max} that changes in sigmoidal steps [Fig. 2(e)]: The first three steps (two hardly perceptible and one of height of ~ 0.2) stand for the density peaks from liquid ordering at the interface, followed by the largest step (~ 0.75) representing the crystallization of the layer. Because of ensemble averaging inherent in DFT, we cannot tell whether single or multiple nucleation takes place. (Simulations with Langevin noise imply multiple 2D nucleation, although, adding noise to Eq. (2) is not free of conceptual difficulties [13].) After a brief transient, the front position Z displays a roughly $Z \propto \tau^{1/2}$ behavior [Fig. 2(f)], indicating a diffusion-controlled growth mechanism, often observed in colloidal systems [14]. We have fitted the function $Z = Z_0 + C(\tau - \tau_0)^{1/2}$ to that part of the position-time relationship, in which diffusion has not yet influenced the liquid density perceptibly at $z = \pm L_z/2$. Here Z_0 is the initial position, C the velocity coefficient, and τ_0 the transient time. The anisotropy of C reflects the differences of the 2D nucleation and step-motion processes on different crystal faces. (Such differences have been studied in detail for crystallization from solutions [15].) We have obtained qualitatively similar results for the hcp and fcc faces.

The C values presented in Table I can be directly compared, as they correspond to essentially the same driving force. The bcc, hcp, and fcc sequences for the growth rates are $C_{111} > C_{100} > C_{110}$, $C_{11\bar{2}0} > C_{10\bar{1}0} > C_{0001}$ and $C_{110} > C_{100}$. We were unable to determine the growth rate of the fcc {111} face, as hcp {0001} has started to grow on it. The close-packed hexagonal interfaces grow far slower than those more corrugated on the atomistic scale. We find that C increases with n_0 [Fig. 2(g)].

There appears a general lack of experimental data for the anisotropy of diffusion-controlled growth of monatomic bcc, hcp, and fcc crystals in single component systems.

TABLE I.   Velocity coefficient C for various interfaces of the bcc, fcc, and hcp structures at $n_0 = -0.04$.

Structure	{100}	{110}	{111}
bcc	0.824 ± 0.002	0.474 ± 0.005	0.948 ± 0.003
fcc	0.916 ± 0.002	0.948 ± 0.002	-
	{10$\bar{1}$0}	{11$\bar{2}$0}	{0001}
hcp	0.228 ± 0.002	0.940 ± 0.002	0.096 ± 0.002

A few examples for the analogous growth of faceted crystals from solutions: The velocity ratio $v_{100}/v_{110} \sim 2.3$ for ^{3}He crystals (bcc) [16], is close to the present ~ 1.7–2.7, while the ratio $v_{10\bar{1}0}/v_{0001} \sim 2.8$ observed for Ca(OH)$_2$ (hexagonal but not hcp) [17] accords reasonably with our ~ 2.4 for hcp; however, this agreement might be fortuitous.

The MD simulations indicate a relatively small kinetic anisotropy for the bcc structure, and the sequence of growth velocities varies with the applied potential [1], although usually $v_{100} > v_{110}$ as here. The MD sequence for the hcp structure (Mg) [1] agrees with the PFC result; however, the anisotropy is smaller. Simulations for the fcc structure (Lennard-Jones, Ni, Ag, Au, Cu, and Fe) [1] indicate that the fastest and lowest growth rates apply for the {100} and {111} orientations. The ratio v_{100}/v_{110} varies in the range of 1.2–1.8, as opposed to the PFC result $C_{100}/C_{110} = 0.97$ obtained at $n_0 = -0.04$. These differences are attributable to the facts that unlike in MD simulations, we have diffusion-controlled growth here, and the MD simulations refer to materials of low melting entropy ($S_f \sim k_B$), whose crystal-liquid interface extends to 4–5 atomic layers, whereas with the present model parameters the PFC realizes a sharp interface.

Finally, we investigate how phase selection is influenced by a foreign substrate of sc structure. The lattice constant a_0, has been varied in a range that incorporates the interatomic distance of the bulk fcc structure (8.204) and the lattice constant of the bulk bcc phase (9.021). With these choices the {100} face of sc is commensurable with the {100} faces of the bulk fcc and bcc structures, respectively. This scenario is analogous to depositing colloidal particles on a square-patterned substrate and also allows us to explore how stress influences the growth rate.

The structure of the crystals that grew in our simulations on the {100} face of the sc substrate, is body-centered tetragonal (bct). The axial ratio c/a varies continuously with a_0 [Fig. 3(a)], where c and a are the lattice constants of the bct structure perpendicular and parallel to the surface of the substrate, respectively. At the appropriate a_0 values, we observe the fcc and bcc structures. These find-
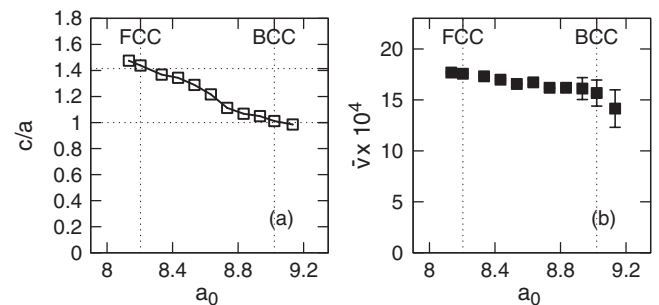

FIG. 3.   Heteroepitaxy in the PFC model: (a) Axial ratio c/a of the bct structure, and (b) the average growth rate ($\bar{v}$) vs the lattice constant (a_0) of the substrate. Bars denote the scattering of $\bar{v}$ due to the variation of the front position Z.

ings show that phase selection can be controlled via the structure of the substrate. Indeed, electrophoretic deposition of a charged polymer colloid on flat substrates with appropriate square-patterned holes produces both the fcc and the bcc structures [18].

The average growth rate ($\bar{v} = \bar{Z}/\tau$) interpolates roughly linearly between the values for the fcc and bcc structures [Fig. 3(b)]. While on the fcc side a planar growth front is seen, for $a_0 > 8.8$ a rough surface composed of pyramids (bound by {110} and/or {111} facets for bcc) evolves presumably as a result of coupled Mullins-Sekerka–Asaro-Tiller-Grinfeld- (MS-ATG-) type instabilities expected in the stress-field the substrate generates in heteroepitaxy [19], probably further enhanced by faceting due to the anisotropy of the interfacial free energy [20]. The instability is reflected in the spatial variation of the average growth rate [see bars in Fig. 3(b)]. The occurrence of the instability on the bcc side is attributable to the lower interfacial free energy relative to the fcc side [1]. It is evident that the substrate plays a role, as in its absence a planar front is observed. As expected for a MS-ATG type instability in the absence of thermal gradient, it can be suppressed beyond a higher critical velocity [19]. In the case of $a_0 = 8.933$, this limit falls to $n_0 \approx -0.005$. Work is underway to quantify these phenomena further.

*Also at Department of Physics, Brown University, Providence, RI 02912-1843, USA.

[1] H. E. A. Huitema, B. van Hengstun, and J. P. van der Eerden, J. Chem. Phys. **111**, 10 248 (1999); M. Amini and B. B. Laird, Phys. Rev. Lett. **97**, 216102 (2006); Z. G. Xia et al., Phys. Rev. B **75**, 012103 (2007); Review: M. Asta et al., Acta Mater. **57**, 941 (2009).

[2] T. V. Ramakrishnan and M. Yussouff, Phys. Rev. B **19**, 2775 (1979); W. A. Curtin and N. W. Ashcroft, Phys. Rev. A **32**, 2909 (1985); J. F. Lutsko and G. Nicolis, Phys. Rev. Lett. **96**, 046102 (2006).

[3] S. van Teeffelen, C. N. Likos, and H. Löwen, Phys. Rev. Lett. **100**, 108302 (2008).

[4] K. R. Elder et al., Phys. Rev. Lett. **88**, 245701 (2002); Phys. Rev. B **75**, 064107 (2007); J. Berry, K. R. Elder, and M. Grant, Phys. Rev. E **77**, 061506 (2008).

[5] Equation (2) has been solved in a dimensionless form on a rectangular grid with periodic boundary condition, using a semi-implicit spectral method based on operator splitting [see G. Tegze et al., J. Comput. Phys. **228**, 1612 (2009)]. The dimensionless time and spatial steps have been $\Delta x = 1$ and $\Delta \tau = 1$. Our computations are consistent with the canonical (N, V, T) ensemble.

[6] V. J. Anderson and N. W. Lekkerkerker, Nature (London) **416**, 811 (2002); A. Yethiraj and A. van Blaaderen, Nature (London) **421**, 513 (2003); H. J. Schöpe, G. Bryant, and W. van Megen, Phys. Rev. Lett. **96**, 175701 (2006).

[7] $\Delta \omega_X = f_X(n_X) - \partial f_L/\partial n(n_0)[n_X - n_0] - f_L(n_0)$, where n_X is the crystal density maximizing the driving force.

[8] E. B. Sirota et al., Phys. Rev. Lett. **62**, 1524 (1989).

[9] The respective sizes of the simulation box were: (i): $L_x = L_y = L_z = 300\Delta x$ $(N \sim 7 \times 10^4$ particles). (ii): $L_z = 1024\Delta x$, while L_x and L_y have been chosen commensurately with the atomic arrangement of the actual face (L_x and L_y are $\sim L_z/5$; $N \sim 1.2 \times 10^5$). This enabled us to grow stress-free perfect crystals. (iii): $L_z = 500\Delta x$, $L_x = L_y = 30a_0 \sim L_z/2$ $(N \sim 10^5)$.

[10] In the single-mode approximation, the reduced number densities for the crystals are bcc: see K. A. Wu and A. Karma, Phys. Rev. B **76**, 184107 (2007), fcc: $n = 8A\{\cos(qx)\cos(qy)\cos(qz)\}$, and sc: $n = 2A\{\cos(qx) + \cos(qy) + \cos(qz)\}$. For hcp, we have used a simple ansatz: $n = A\{\cos(2qy/\sqrt{3}) + \cos(qx - qy/\sqrt{3}) - \cos(2\pi/3 - qx + qy/\sqrt{3}) + \cos(qx + qy/\sqrt{3}) - \cos(-4\pi/3 + qx + qy/\sqrt{3}) - \cos(-2\pi/3 + 2qy/\sqrt{3})\}\cos[(\sqrt{3}/\sqrt{8})qz]$. Here $q = 2\pi/a$. The lattice constant a and the amplitude A have been determined by analytic minimization of the free energy.

[11] D. V. Talapin et al., Adv. Mater. **17**, 1325 (2005); J. D. Woodward et al., J. Phys. Chem. B **110**, 19 456 (2006).

[12] R. L. Davidchack and B. B. Laird, J. Chem. Phys. **108**, 9452 (1998).

[13] U. M. B. Marconi and P. Tarazona, J. Chem. Phys. **110**, 8032 (1999).

[14] A. P. Gast and Y. Monovoukas, Nature (London) **351**, 553 (1991); K. Schätzel and B. J. Ackerson, Phys. Rev. E **48**, 3766 (1993); W. B. Russel et al., Langmuir **13**, 3871 (1997); S. I. Henderson and W. van Megen, Phys. Rev. Lett. **80**, 877 (1998).

[15] A. A. Chernov, Contemp. Phys. **30**, 251 (1989).

[16] V. Tsepelin et al., Phys. Rev. Lett. **88**, 045302 (2002).

[17] V. S. Harutyunyan et al., J. Mater. Sci. **44**, 962 (2009).

[18] N. V. Dziomkina, M. A. Hempenius, and J. G. Vancso, Adv. Mater. **17**, 237 (2005).

[19] I. Durand et al., Phys. Rev. Lett. **76**, 3013 (1996).

[20] T. Savina et al., Phys. Rev. E **67**, 021606 (2003).